Organic Electronics 12 (2011) 686–693

Contents lists available at ScienceDirect

Organic Electronics

journal homepage: www.elsevier.com/locate/orgel

Low-temperature formation of self-assembled 1,5-diaminoanthraquinone nanofibers: Substrate effects and field emission characteristics

Kuo-Jung Huang [a], Yu-Sheng Hsiao [b,*], Wha-Tzong Whang [a,*]

[a] Department of Materials Science and Engineering, National Chiao Tung University, Hsinchu 30010, Taiwan, ROC
[b] Research Center for Applied Sciences, Academia Sinica, Taipei 11529, Taiwan, ROC

ARTICLE INFO

Article history:
Received 11 October 2010
Received in revised form 11 January 2011
Accepted 12 January 2011
Available online 23 February 2011

Keywords:
DAAQ
Self-assemble
Nanofibers
Small organic molecules
Field emission

ABSTRACT

In this study, we used thermal evaporation with a low sublimation temperature (42 °C) to deposit 1,5-diaminoanthraquinone (DAAQ) in various morphologies—including nanorods, nanocornerstones, and nanofibers—onto various substrates. Three major factors influenced the growth of vertically aligned DAAQ nanofibers on the electrodes: a low water contact angle (WCA) for the substrate and intermolecular hydrogen bonding and π–π interactions between the DAAQ molecules. On Au and Ti substrates (low-WCA), the DAAQ nanofibers **DAAQ-Au** and **DAAQ-Ti**, respectively, possessed great verticality and high aspect ratios; they also exhibited field emission characteristics, with maximum emission current densities of 0.31 and 0.65 mA/cm^2, respectively, at an applied electric field of 12 V/μm. The turn-on electric fields for producing a current density of 10 μA/cm^2 were 8.5 V/μm for **DAAQ-Au** and 8.25 V/μm for **DAAQ-Ti**. From the slopes of Fowler–Nordheim plots, we calculated the field enhancement factors (β) of **DAAQ-Au** and **DAAQ-Ti** to be 447 and 831, respectively. Field emission stability studies revealed that the DAAQ nanofibers possessed outstanding anti-degrading capability. The emission current did not decrease, but rather increased slightly, after 3000 s. Given the advantages of this simple low-temperature process and the impressive anti-degrading field emission characteristics, such DAAQ nanofibers have great potential for use in various electronics applications (e.g., as organic field emitters).

1. Introduction

Nanostructures based small organic molecules have become the focus of intensive research efforts because of their unique applications in nanoscale devices [1–3]. One-dimensional (1D) organic nanostructures, including nanorods, nanofibers, nanowires, and nanotubes, can be fabricated using a wide range of methods; they often exhibit unique material properties that make them suitable for use in organic electronics applications (e.g., solar cells [4–7], chemical vapor sensors [8], field emitters [9–15]) and in various optoelectronic devices [16–19]. Recently, several small organic molecules, including tris(8-hydroxyquinolinato) aluminum (Alq_3) [9,13,16,19], anthracene (AN), perylene (PY) [20], coronene [10], copper phthalocyanine (CuPc) [11], and 1,5-diaminoanthraquinone (DAAQ) [8], have been prepared in form of various nanostructures under conditions milder than those used to prepare related nanostructures from inorganic compounds. Because of their suitability for use in inexpensive, low temperature-processed, highly flexible optoelectronic devices, increasing attention is being drawn to the development of nanostructures of small-molecule organic materials.

Several fabrication methods have been reported for the preparation of organic 1D nanostructures [1–3,21]. Nanowires and nanorods have been prepared through thermal evaporation (solid state chemical reactions) [20]

* Corresponding authors. Tel.: +886 2 27898000-21; fax: +886 2 27826680 (Y.S. Hsiao), tel.: +886 35 731873; fax: +886 35 724727 (W.T. Whang).
E-mail addresses: yshsiao@gate.sinica.edu.tw (Y.-S. Hsiao), wtwhang@mail.nctu.edu.tw (W.-T. Whang).

1566-1199/$ - see front matter © 2011 Elsevier B.V. All rights reserved.
doi:10.1016/j.orgel.2011.01.010

at high temperatures (up to 280 °C). Solution processing of nanorods has been employed using a microemulsion route assisted by surfactants [19]. Self-polymerization and self-assembly process has been developed for production of supramolecular nanomaterials [22]. Thermal evaporation of nanotubes and nanotube junctions onto metal catalysts has been performed at 340 °C under a flow of Ar gas [23]. Vapor condensation has been used to prepare nanowires [9] and nanoparticles [24] under Ar atmospheres at temperatures of over 400 °C with the substrate placed under a N_2-cooled trap. Zhao et al. applied neutral aluminum oxide (or silica gel) in the adsorbent-assisted physical vapor deposition of nanoribbons and nanowires [25,26]. Vacuum sublimation, a form of vapor-phase deposition, has also been applied to the preparation of nanostructures, particularly for fabricating 1D organic nanofibers for organic field emission devices [10–12]. We have previously applied high vacuum processing to fabricate nanostructures with highly uniform distributions on targeting substrates, without the need for catalysts or high temperatures. Such simple one-step approaches not only eliminate the effects of impurities but also potentially lower the fabrication temperature.

Recent investigations of DAAQ-based optoelectronic devices, such as chemical sensors [8], optical waveguides [27], and organic solar cells [28], have led to a rapid development of DAAQ fabrication technologies. Zhao et al. [27] recently reported that this organic dye prefers to undergo vertical deposition on substrates having high surface energies (SEs) and hydrophilic domains. In this present study, we synthesized 1D DAAQ nanofibers through vacuum sublimation on selected substrates. We characterized these 1D DAAQ nanofibers using scanning electron microscopy (SEM) and high-resolution transmission electron microscopy (HRTEM). From investigations of the morphologies of DAAQ thin films formed on different substrates, we selected electrodes suitable for the vertical deposition of DAAQ nanofibers. To determine the practicality of employing DAAQ nanofibers as cathode materials in field emission devices, we evaluated their field emission characteristics using a vacuum emission measurement (VEM) system.

Stabilized by intermolecular hydrogen bonding and π–π interactions, DAAQ self-assembles onto substrates to form vertically out-of-plane nanostructures. Analogous to organic vapor-phase deposition (OVPD), the vacuum sublimation of small organic molecules is also a vapor-solid (VS) process. Because sublimation proceeds at lower temperatures in higher vacuums, relative to those used for OVPD, its use opens up a new area of study and potentially increases the applications of organic small molecules in flexible electronic devices.

2. Experimental

Commercially available DAAQ powder (purity: 92%; Tokyo Chemical Industry) and 1,1,1,3,3,3-hexamethyldisilazane (HMDS; Lancaster), for Si surface treatment, were used as received without further purification.

DAAQ films were deposited on various substrates (Ag, Al, Au, Ni, Si, Ti) using a thermal evaporator operated at a base pressure of 6×10^{-6} torr. The metal substrates were prepared by depositing metal films onto Si (1 0 0) substrates using an electron beam (E-beam) evaporator. Prior to E-beam evaporation of each metal thin film, a Ti layer (thickness: 200 Å) was deposited on the bare Si substrate as an adhesion layer. Without breaking the vacuum, a thin layer of Ag, Al, Au, Ni, or Ti (thickness: 1000 Å) was then deposited. The entire Si substrate was treated with HMDS vapor and then cured at 160 °C for 0.5 h, and the surface chemistry of the Si substrate was modified through the formation of a self-assembled monolayer of HMDS.

DAAQ nanostructure films were formed on the various substrates while maintaining the substrate temperature at 25 °C. The sublimation of DAAQ was performed at a temperature of 42 °C; the corresponding deposition rate, controlled by a quartz crystal microbalance, was 0.5 Å/s.

Top and cross-sectional views of the morphologies of the DAAQ nanostructure films were surveyed using a JEOL JSM-6500F scanning electron microscope. Ultraviolet–visible (UV–Vis) spectra (250–900 nm) were recorded using a Shimadzu UV-3600 spectrophotometer. Contact angles (CAs) and SEs were determined on each substrate using a Krüss universal surface tester (model GH-100), the geometric mean approximation, and three standard liquids: water (H_2O), diiodomethane (CH_2I_2), and ethylene glycol [$C_2H_4(OH)_2$]. The profiles and fine structure of nanofibers were imaged and analyzed using a JEOL-2010 high-resolution transmission electron microscope and an internal charge-coupled device (CCD) camera. The crystalline of DAAQ nanofibers was characterized by GIXRD, using Bruker D8 system and Cu Kα radiation. The incident angle of the X-ray beam was fixed at 0.2°. The field emission characteristics of the DAAQ nanofibers were determined under a base pressure of 8×10^{-6} torr. Indium tin oxide (ITO) plate glasses were used as anodes, positioned above the substrate surfaces at a distance of 80 μm. The field emission instrument featured a plate-to-plate geometry; the cathode comprised DAAQ nanofibers deposited on Au and Ti substrates (area: 0.06 cm^2). Current density–electric field (J–E) curves of the field emission devices were measured using a Keithley 237 instrument (accuracy: 10^{-13} A). The emission currents of the DAAQ nanofibers were monitored as a function of the sweep bias.

3. Results and discussion

Fig. 1(a) displays the molecular structure of DAAQ. Assemblies of DAAQ molecules feature both intramolecular charge transfer [29] and intermolecular hydrogen bonding [23]. Intramolecular charge transfer occurs between the amino (NH_2) and carbonyl (C=O) groups of the anthraquinone ring; intermolecular hydrogen bonding occurs between the oxygen atoms of the C=O group in one DAAQ molecule and the hydrogen atoms of the NH_2 group in another. For the nonpolar molecule coronene [10] to form 1D nanofibers, molecular stacking occurs mainly through π–π and van der Waals interactions. In the stacking of DAAQ molecules, we suspected that both intra- and intermolecular hydrogen bonds would coexist. In addition to π–π interactions and van der Waals contacts between

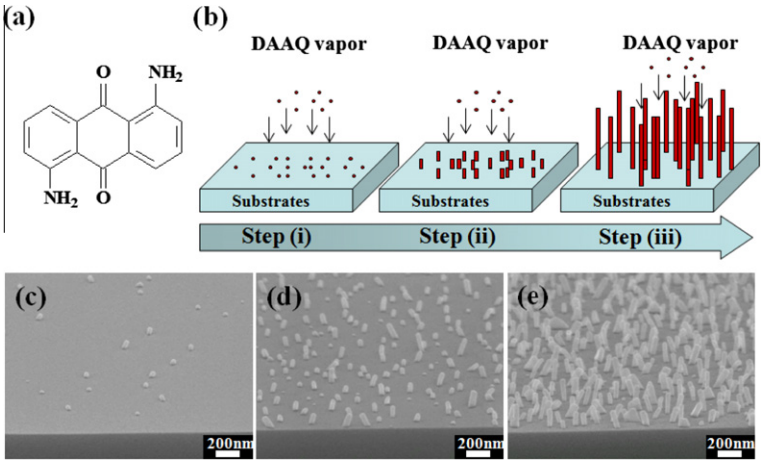

Fig. 1. (a) Chemical structure of DAAQ. (b) Schematic representation of the growth of 1D DAAQ nanofibers through vacuum sublimation. SEM images (cross-sectional view) of DAAQ thin films grown on a Si substrate for (c) 6 s, (d) 10 s, and (e) 60 s at a deposition rate of 0.5 Å/s.

stacking molecules, intermolecular hydrogen bond also plays an important role in 1D self-assembly.

The major advantage of vacuum sublimating DAAQ nanostructure films is the simplicity and accessibility of the process. No catalyst is used and no droplets of catalyst are found at the tips of the nanofibers; therefore, the growth mechanism of DAAQ nanostructure films is presumed to be similar to that of the physical vapor transport method [27]. One strategy for achieving 1D structures, reported by Xia et al. [30], is the use of various templates with 1D morphologies to direct the assembly process. The growth mechanism normally involves three steps (Fig. 1(b)) (i) as the concentration of DAAQ increases, the molecular building blocks begin to aggregate into small nuclei; (ii) these nuclei become seeds for the anisotropic packing of DAAQ molecules; (iii) with a continuous supply of DAAQ, vapor molecules self-assemble to form 1D morphologies with vertically aligned nanostructures on the substrates. In this study, we used vacuum sublimation of DAAQ to construct 1D nanostructures on selected substrates. We investigated the growth mechanism of these DAAQ thin films to develop guidelines for the design of suitable structures for field emitters. Fig. 1(c–e) present cross-sectional SEM images of the early stage (6, 10, and 60 s of deposition at a rate of 0.5 Å/s, respectively) products of the DAAQ nanofibers on a Si wafer. We observe a layer of vertically self-assembled and elongated nanoparticles, which acted as seeds for the anisotropic overgrowth of the nanofibers into columnar structures. Furthermore, varying the deposition time allowed us to adjust the length of the nanofibers on the substrates.

Fig. 2 presents SEM images (top and cross-sectional views) of the DAAQ nanostructure films formed on the Ag, Al, Au, Ni, Si, and Ti substrates. Clearly, the nature of the substrate influenced the morphology of its DAAQ thin film. Fig. 2(a and d) reveal entangled, in-plane, rod-like morphologies for the DAAQ films formed on the Ag and Ni substrates, respectively. In the top-view SEM images in Fig. 2(b, c and e, f) we observe that most of the DAAQ nanofibers grew perpendicularly (slightly slanting) from the substrates to form quasi-arrays. Repulsive forces among nuclei can result in a parallel-displaced conformation, leading to a tilted columnar structure [10,31]. In Fig. 2(c, e, and f), the high-density packing morphologies of the DAAQ nanofibers on the Si and Ti substrates are similar to those on the Au surface. The densities of these nanostructures on all of the substrates ranged from 10^8 to 10^9 cm^{-2} (Table 1). The DAAQ thin films deposited on the Ag and Ni substrates both possessed tilted out-of-plane and in-plane nanorod morphologies, as revealed in their cross-sectional SEM images (insets to Fig. 2(a and d), respectively). The short, tilted nanorods on the Ag surface had a mean radius of 48 nm and a mean length of 226 nm; those on the Ni substrate, however, had larger dimensions (90 and 843 nm, respectively). The DAAQ nanostructures deposited on the Al substrate (inset to Fig. 2(b)) had the largest average radius (100 nm) and length (883 nm); we suspect these oversized nanostructures comprised three or four nanofibers aggregated together in the form of nanocornerstones. In contrast, the DAAQ molecules packed on the Au, Si, and Ti substrates to present an out-of-plane morphology with uniform arrangement; these nanofibers had average lengths of 427, 794, and 587 nm, respectively (insets to Fig. 2(c, e, and f), respectively). The mean radii of these nanofibers, featuring smooth surfaces, ranged from 27 to 35 nm. The lengths of the nanofibers on these substrates could be adjusted by varying the deposition time. Table 1 summarizes the mean lengths (L), radii (r_m), and nanostructural types of the DAAQ assemblies deposited on the various substrates. The aspect ratios (ARs), defined as

$$\mathrm{AR} = L/r_m \tag{1}$$

of the 1D DAAQ nanofibers deposited on the Au, Si, and Ti substrates were 12.6, 29.4, and 16.8, respectively. The high ARs of these DAAQ nanofibers suggest that they are potentially applicable nanostructures for use as organic field emitters.

The selective growth of vertical DAAQ nanowires generally occurs through preferential deposition on geometrical

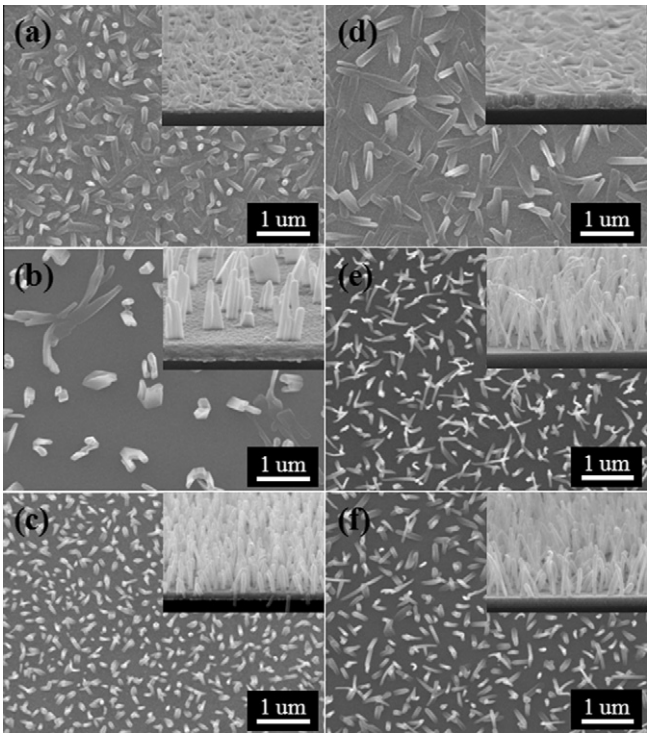

Fig. 2. SEM images (top view) of DAAQ thin films deposited on (a) Ag, (b) Al, (c) Au, (d) Ni, (e) Si, and (f) Ti substrates. Insets are the cross-sectional SEM images.

Table 1
Mean lengths (L), mean radii (r_m), ARs, nanostructure types, and distributions for the DAAQ thin films deposited on various substrates.

Substrate	Mean length (nm)	Mean radius (nm)	AR	Nanostructure type	Distribution ($1/cm^2$)
Ag	226	48	4.7	Nanorod	2.4×10^9
Al	883	100	8.8	Nanocornerstone	2.1×10^8
Au	427	34	12.6	Nanofiber	2.5×10^9
Ni	843	90	9.4	Nanorod	5.8×10^8
Si	794	27	29.4	Nanofiber	1.6×10^9
Ti	587	35	16.8	Nanofiber	1.6×10^9

chemically modified surfaces; for example, substrates featuring sharp tips or edges, silica beads, or hydrophilic domains [27]. To realize the effects of CAs and to select appropriate metals for use as electrodes for potential applicability in organic field emission, we selected Ag, Au, Al, Ni, Si, and Ti as substrates and investigated the morphologies of the DAAQ nanostructure films formed on these surfaces. Table 2 summarizes the CAs of the various substrates and their SEs, calculated using the Owens and Wendt method [32]. The water contact angles (WCAs) of the Ag, Al, and Ni substrates were 96.1°, 96.7°, and 100.9°, respectively, making them hydrophobic substrates. The majority of DAAQ molecules deposited on these substrates formed flat and entangled structures. In contrast, the DAAQ molecules deposited on the Au, Si, and Ti surfaces extended perpendicularly from the substrates, which had WCAs of 81.8°, 59.7°, and 78.8°, respectively (i.e., hydrophilic substrates). Therefore, it appears that the preferred growth of 1D vertical DAAQ nanofibers requires hydrophilic, rather than hydrophobic, surfaces. This result is similar to those reported by Zhao et al. [27] who studied the effect using UV–Vis absorption spectroscopy. Next, we performed surface treatment of the Si substrate to confirm our

Table 2
CAs and SEs of various substrates.

Substrate	CA (°)			SE[b] (mJ/m^2)
	H_2O	CH_2I_2	$C_2H_4(OH)_2$	
Ag	96.1	52.7	66.5	34.8
Al	96.7	49.5	72.8	35.0
Au	81.8	19.9	56.2	45.1
Ni	100.9	39.5	69.9	46.4
Si	59.7	48.1	38.2	41.3
Ti	78.8	33.5	57.0	39.0
SiH[a]	88.5	58.5	69.9	27.6

[a] Sample obtained after the bare Si substrate had been treated with HMDS vapor and annealed at 160 °C for 30 min.
[b] Calculated using the Owens method from the geometric mean approximation (GMA) measurements of the static CAs of H_2O, CH_2I_2, and $C_2H_4(OH)_2$.

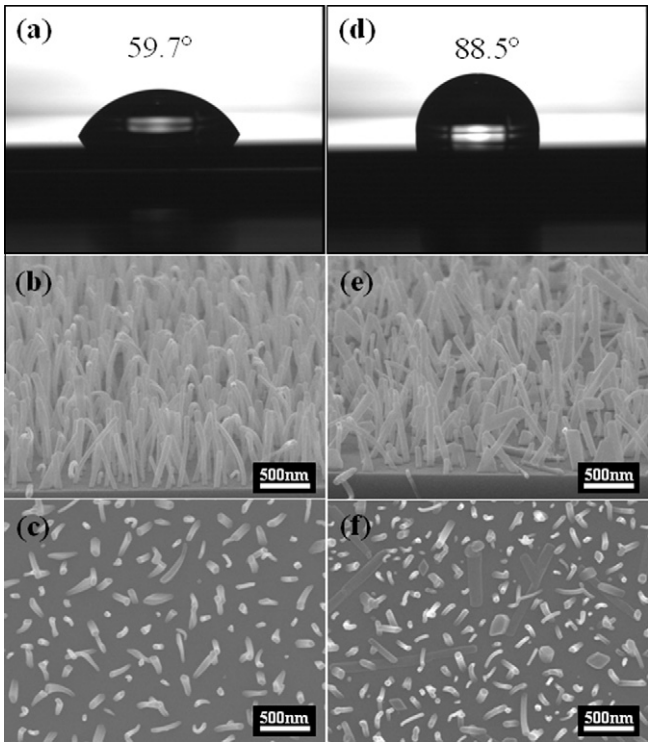

Fig. 3. (a, d) Photographs of water droplets on the (a) bare Si substrate (WCA: 59.7°) and (d) HMDS-treated SiH substrate (WCA: 88.5°). (b, c, e, f) SEM images of the DAAQ structures formed on the (b, c) bare Si and (e, f) SiH substrates; (b, e) cross-sectional views; (c, f) top views.

hypothesis. Fig. 3(a and d) present images of water droplets on the surfaces of bare Si and HMDS-treated Si (SiH), respectively; the WCAs were 59.7° and 88.5°, respectively. We suspect that the greater WCA for the SiH substrate resulted from a reduction in the density of interfacial trapping states and a lowering of the SE. Fig. 3(b and c) display SEM images of the DAAQ thin films deposited on the bare Si surface; as before, the structures extend away from the substrate. In contrast, some of the DAAQ nanofibers were deposited in-plane and entangled on the SiH substrate (Fig. 3(e and f)). This finding confirms that a low-WCA surface endows a preference for vertical deposition of 1D DAAQ nanofibers.

Fig. 4(a and c) present TEM images of the DAAQ nanofibers formed on the Au and Ti substrates, respectively; these nanofibers were very smoothly faceted and uniform in length. High-resolution TEM images of single nanofibers revealed (Fig. 4(b and d)) indistinct lattice fringe spacing. We suspect that the DAAQ molecules were oriented in short-range order at the edges of the nanofibers, but entangled randomly within the nanofibers. The selected area electron diffraction (SAED) pattern in the inset to Fig. 4(a) features only amorphous rings, rather than distinct diffractive spots, suggesting that an insignificant degree of crystallinity was responsible for the isotropic and randomly oriented molecules. Similarly, the electron diffraction pattern in the inset to Fig. 4(c) also reveals the amorphous features of the DAAQ molecules deposited on the Ti substrates. In addition, these HRTEM images do not reveal the presence of any metal catalysts at the tips of the fibers, confirming that the growth mechanism was different from that of carbon nanotubes (CNTs) [33]. In order to understand the lattice differences in our system, the XRD patterns of the DAAQ commercial powders and nanofiber arrays were used to further study (Fig. 4(e)). Although the DAAQ nanofiber arrays feature lower peak intensity than the commercial powders, the relative percentages of (1 0 0), (1 0 2) and (1 1 2) lattice planes show some changes. Comparison of our results with the previous report of DAAQ nanowires [8], the DAAQ nanofiber arrays (formed by vacuum sublimation in low-temperature process) also prefer to grow in the orientation of (1 0 0) lattice plane.

To determine the differences in energy levels between the electrodes and the DAAQ materials for potential field emission applications, we used photoelectron spectroscopy in air (PESA; Fig. 5(a)) and UV–Vis spectroscopy (Fig. 5(b)) to measure the energy levels of DAAQ. When we bombarded our surface materials under a slowly increasing amount of UV light, photoelectrons were emitted from the surface (from a depth of several to hundred angstroms) at a certain energy level, due to the photoelectron effect. These emitted photoelectrons were then counted by a detector and open counter. Using this approach, the valence band [highest occupied molecular orbital (HOMO)] of DAAQ obtained through linear fitting from the PESA data was 5.60 eV relative to the vacuum level. The UV–Vis absorption spectra of the DAAQ films revealed an absorption band in the region 300–800 nm. From the on set wavelength at 614 nm, we derived an energy gap

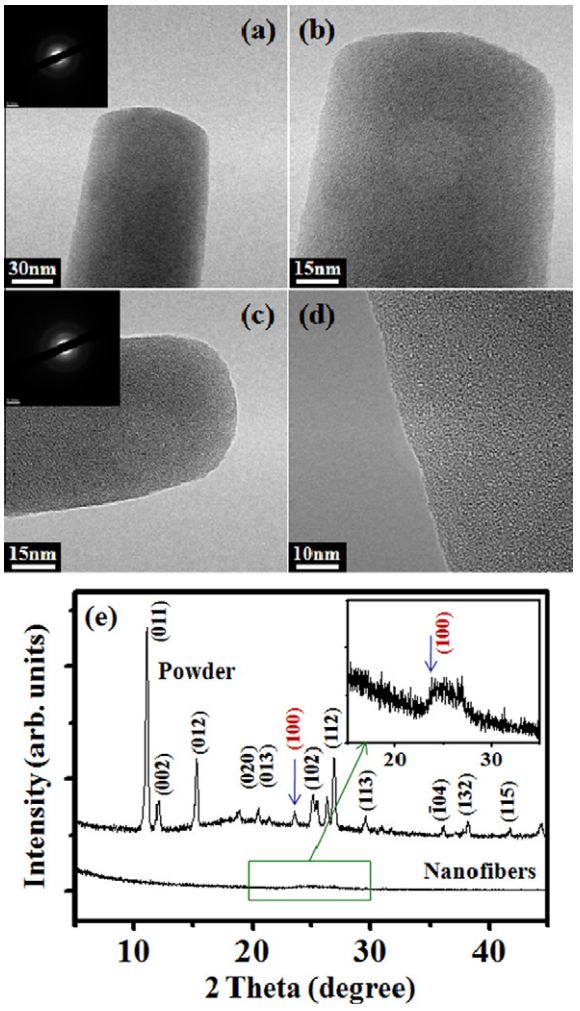

Fig. 4. (a) HRTEM image of a single DAAQ nanofiber formed on the Au substrate; inset: corresponding SAED pattern. (b) Magnified image of the nanofiber in (a). (c) HRTEM image of a single DAAQ nanofiber formed on the Ti substrate; inset: corresponding SAED pattern. (d) HRTEM image of the smooth surface of a single nanofiber. (e) XRD patterns of DAAQ commercial powder (top) and nanofiber arrays (bottom). Inset: magnified XRD pattern of DAAQ nanofiber arrays.

for the DAAQ of 2.02 eV. From this value, we estimated the energy of the conduction band [lowest unoccupied molecular orbital (LUMO)] to be 3.58 eV. Fig. 5(c and d) provide a schematic energy level diagram; the HOMO and LUMO states of DAAQ were 5.60 eV and 3.58 eV, respectively; the work functions of Au and Ti, for use as cathode substrates, were 5.1 and 4.33 eV, respectively. Therefore, electrons injected from the Au substrate into the LUMO state of the DAAQ layer must conquer a larger energy gap than those injected from the Ti substrate.

We examined the field emission properties of the DAAQ nanofibers using a parallel-plate configuration with the spacing of 80 μm in a vacuum chamber at a pressure of 8×10^{-6} torr. The anode ITO glass was connected to the source monitor unit (SMU) of a Keithley 237 instrument; the cathode of Au and Ti substrates were grounded. Fig. 6 displays the field emission characteristics (J–E curve) of the DAAQ nanofibers deposited on the Au (**DAAQ-Au**) and Ti (**DAAQ-Ti**) substrates. The turn-on fields (defined as the applied field required for a current density of 10 μA/cm^2) of **DAAQ-Au** and **DAAQ-Ti** were 8.5 and 8.25 V/μm, respectively; at an applied field of 12 V/μm, the maximum current densities were 0.31 and 0.65 mA/cm^2, respectively. The dependence of the emission current of a field emitter on the applied field is described by the Fowler–Nordheim (FN) equation [34]:

$$ln\left(\frac{J}{E^2}\right) = \ln\left(\frac{A\beta^2}{\phi}\right) + \left(\frac{-B\phi^{3/2}}{\beta}\right)\left(\frac{1}{E}\right) \quad (2)$$

where A and B are constants (1.54×10^{-6} A eV/V^2 and 6.83×10^3 V/eV$^{3/2}$/μm, respectively), J is the current density, E is the applied field, and ϕ is the local work function of the emitter material. By plotting $\ln(J/E^2)$ versus $1/E$, the slope of the line of best fit can be used to deduce the field enhancement factor (β):

$$\beta = -\frac{B\phi^{3/2}}{S} \quad (3)$$

where S is the slope of the FN plot. According to FN theory, β is strongly dependent on the geometric structure of the field emitter. The linear FN plots in the insets to Fig. 6(a and b) reveal that the J–E characteristics of the DAAQ nanofibers followed the FN field emission mechanism. The slopes of FN plots for **DAAQ-Au** and **DAAQ-Ti** were −103.5 and −55.67, respectively. Because the LUMO energy level (ϕ) of DAAQ was 3.58 eV, we estimated the values of β of **DAAQ-Au** and **DAAQ-Ti** to be 447 and 831, respectively. To understand why these values of β differed so dramatically, we must consider the effect of the geometry of the nanofibers. Tarntair et al. [35] reported that the field enhancement factor β could be approximated by the length-to-radius ratio of the 1D nanostructure, expressed as

$$\beta = \frac{l}{r} \quad (4)$$

where r is the radius of curvature of the tip and l is the length of the nanofiber. This equation suggests that emitters having longer lengths and smaller radii, resulting in larger values of β, would have better field emission characteristics. Because our low-WCA surfaces (Au and Ti) favored DAAQ molecules self-assembling into standing nanofibers and because the value of β of **DAAQ-Ti** was greater than that of **DAAQ-Au**, we suspected that the higher AR of the DAAQ nanofibers deposited on Ti would be superior, to those formed on Au, for use in field emission devices. Cho et al. [36] reported the effective radius (r_e) of an effective area at the tips of their Alq_3 nanostructural thin film; the calculated radius (r_e = 2.07 nm) was smaller than the measured radius (r_m = 40 nm). The DAAQ nanofibers of **DAAQ-Au** and **DAAQ-Ti** had effective radii of 0.96 and 0.7 nm, respectively (Table 3). From the differences between the values of r_m (34 nm for **DAAQ-Au**; 35 nm for **DAAQ-Ti**) and r_e, we suspect that the electrons were emitted from a localized area at the tip of a nanofiber, rather than from the entire measured area of the nanofiber. From the viewpoint of the energy levels, Fig. 5(c and d) reveal

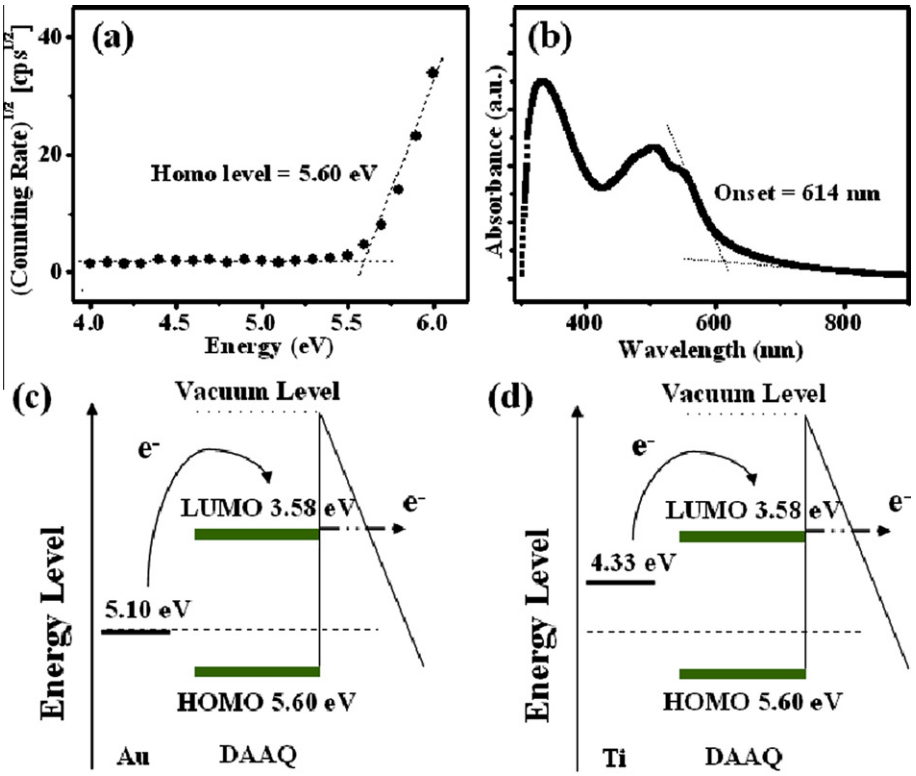

Fig. 5. (a) PESA analysis of the DAAQ thin films. (b) UV–Vis absorption spectra of DAAQ thin films. (c, d) Schematic representations of the energy levels and electrons field emitting through the DAAQ nanofibers of the (c) Au-DAAQ and (d) Ti-DAAQ contacts.

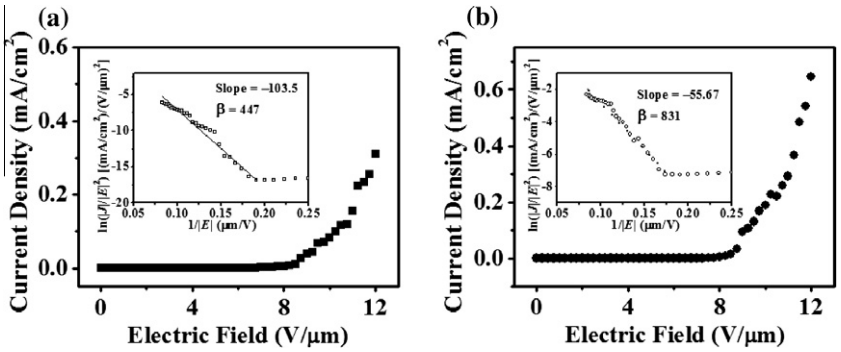

Fig. 6. Field emission *J–E* curves of (a) **DAAQ-Au** and (b) **DAAQ-Ti**. Insets: Corresponding FN plots.

Table 3
Values of $E_{turn\text{-}on}$, slopes of FN plots, field emission enhancement factors (β), and effective radii (r_e) for the DAAQ nanofibers.

Substrate	$E_{turn\text{-}on}$ (V/μm)	Slope	β	r_e (nm)
Au	8.50	−103.50	447	0.96
Ti	8.25	−55.67	831	0.70

that the work function (5.1 eV) of Au was much higher than that (4.33 eV) of Ti; therefore, the energy barrier (1.52 eV) at the Au-DAAQ interface was larger than that (0.75 eV) at the Ti-DAAQ contact. These energy barriers limited the injection of electrons from the conducting substrates to organic nanofibers; consequently, a higher applied field was required to reach the same level of emission current.

We performed stability tests of our DDAQ nanofibers under an applied field of 11 V/μm for 3000 s. The calculated mean current densities were ca. 0.07 mA/cm^2 for **DAAQ-Au** (Fig. 7(a)) and 0.19 mA/cm^2 for **DAAQ-Ti** (Fig. 7(b)), with perturbations of less than one order. In addition, we observed a slowly increasing **DAAQ-Ti** emission current over time and two apparent increasing **DAAQ-Au** emission currents from 150 to 250 s and from

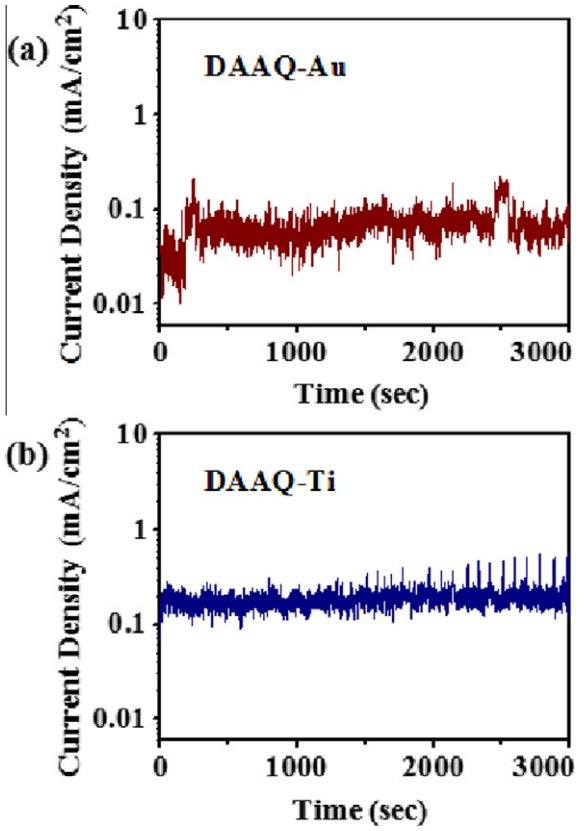

Fig. 7. Emission current stability plots recorded at a constant voltage for 3000 s: (a) **DAAQ-Au**; (b) **DAAQ-Ti**.

2440 to 2540 s. The latter presumably arose from a training effect [37,38]; that is, contaminants were expelled from the nanofibers after an adapted biasing on the nanofibers for a period of time. Thus, the organic semiconductor sustained a stable field emission current, without any decay, during the measurement period, demonstrating that DAAQ organic nanofibers have great potential for use in cold field electron-emitting devices.

4. Conclusions

By using DAAQ as a starting material, we prepared vertical organic nanofibers through low-temperature (42 °C) vacuum sublimation. The morphologies of the structures formed from the DAAQ molecules were controlled by the surface properties of the substrates, with vertically aligned 1D DAAQ structures growing preferentially on low-WCA surfaces, such as Au, Si, and Ti. The DAAQ nanofibers exhibited unique field emission characteristics and followed FN behavior. The maximum emission current densities of **DAAQ-Au** and **DAAQ-Ti** were 0.31 and 0.65 mA/cm^2 when biased at 960 V (E = 12 V/μm), respectively. The field enhancement factors β of the DAAQ nanofibers on the Au and Ti substrates were 447 and 831, respectively. In field emission stability tests, the field emission current was stable, without any decay, during the duration of the measurements. The stability of the emission current and the simplicity of the synthetic process suggest that this method of fabricating vertically aligned DAAQ nanofibers is suitable for application in the fabrication of electron-emitting devices.

Acknowledgment

We thank for National Science Council (Project NSC 98-2221-E-009-021-MY3), ROC, for financial support.

References

[1] A.B. Djurišić, A.M.C. Ng, K.Y. Cheung, M.K. Fung, W.K. Chan, J. Mater. Sci. Technol. 24 (2008) 563.
[2] Y.S. Zhao, H. Fu, A. Peng, Y. Ma, D. Xiao, J. Yao, Adv. Mater. 20 (2008) 2859.
[3] Y.S. Zhao, H. Fu, A. Peng, Y. Ma, Q. Liao, J. Yao, Acc. Chem. Res. 43 (2010) 409.
[4] F. Yang, M. Shtein, S.R. Forrest, J. Appl. Phys. 98 (2005) 014906.
[5] F. Yang, S.R. Forrest, Adv. Mater. 18 (2006) 2018.
[6] R.R. Lunt, J.B. Benziger, S.R. Forrest, Appl. Phys. Lett. 90 (2007) 181932.
[7] Y.S. Hsiao, W.T. Whang, S.C. Suen, J.Y. Shiu, C.P. Chen, Nanotechnology 19 (2008) 415603.
[8] Y.S. Zhao, J. Wu, J. Huang, J. Am. Chem. Soc. 131 (2009) 3158.
[9] J.J. Chiu, C.C. Kei, T.P. Perng, W.S. Wang, Adv. Mater. 15 (2003) 1361.
[10] S.C. Suen, W.T. Whang, B.W. Wu, Y.F. Lai, Appl. Phys. Lett. 84 (2004) 3157.
[11] S.C. Suen, W.T. Whang, F.J. Hou, B.T. Dai, Org. Electron. 7 (2006) 428.
[12] S.C. Suen, W.T. Whang, F.J. Hou, B.T. Dai, Org. Electron. 8 (2007) 505.
[13] C.P. Cho, T.P. Perng, Org. Electron. 11 (2010) 115.
[14] H. Liu, Q. Zhao, Y. Li, Y. Liu, F. Lu, J. Zhuang, S. Wang, L. Jiang, D. Zhu, D. Yu, L. Chi, J. Am. Chem. Soc. 127 (2005) 1120.
[15] S. Cui, Y. Li, Y. Guo, H. Liu, Y. Song, J. Xu, J. Lv, M. Zhu, D. Zhu, Adv. Mater. 20 (2008) 309.
[16] J.J. Chiu, W.S. Wang, C.C. Kei, C.P. Cho, T.P. Perng, P.K. Wei, S.Y. Chiu, Appl. Phys. Lett. 83 (2003) 4607.
[17] Y.S. Zhao, J. Xu, A. Peng, H. Fu, Y. Ma, J. Yao, Adv. Mater. 20 (2008) 1661.
[18] Y.S. Zhao, H. Fu, F. Hu, A.D. Peng, J. Yao, Adv. Mater. 19 (2007) 3554.
[19] W. Chen, Q. Peng, Y. Li, Adv. Mater. 20 (2008) 2747.
[20] H. Liu, Y. Li, S. Xiao, H. Gan, T. Jiu, H. Li, L. Jiang, D. Zhu, D. Yu, B. Xiang, Y. Chen, J. Am. Chem. Soc. 125 (2003) 10794.
[21] S. Cui, H. Liu, L. Gan, Y. Li, D. Zhu, Adv. Mater. 20 (2008) 2918.
[22] H. Gan, H. Liu, Y. Li, Q. Zhao, Y. Li, S. Wang, T. Jiu, N. Wang, X. He, D. Yu, D. Zhu, J. Am. Chem. Soc. 127 (2005) 12452.
[23] H. Liu, Y. Li, S. Xiao, H. Li, L. Jiang, D. Zhu, B. Xiang, Y. Chen, D. Yu, J. Phys. Chem. B 108 (2004) 7744.
[24] J.J. Chiu, W.S. Wang, C.C. Kei, T.P. Perng, Appl. Phys. Lett. 83 (2003) 347.
[25] Y.S. Zhao, C.A. Di, W. Yang, G. Yu, Y. Liu, J. Yao, Adv. Funct. Mater. 16 (2006) 1985.
[26] Y.S. Zhao, D. Xiao, W. Yang, A. Perng, J. Yao, Chem. Mater. 18 (2006) 2302.
[27] Y.S. Zhao, P. Zhan, J. Kim, K. Sun, J. Huang, ACS Nano 4 (2010) 1630.
[28] H. Derouiche, V. Djara, Sol. Energy Mater. Sol. Cells 83 (2004) 125.
[29] G. Suganthi, C. Meenakshi, V. Ramakrishnan, J. Fluoresc. 20 (2010) 95.
[30] Y.N. Xia, P.D. Yang, Y.G. Sun, Y.Y. Wu, B. Mayers, B. Gates, Y.D. Yin, F. Kim, H.Q. Yan, Adv. Mater. 15 (2003) 353.
[31] J.D. Wright, Molecular Crystals, second ed., Cambridge University Press, 1995. p. 22.
[32] D.K. Owens, R.C. Wendt, J. Appl. Polym. Sci. 13 (1969) 1741.
[33] V. Vinciguerra, F. Buonocore, G. Panzera, L. Occhipinti, Nanotechnology 14 (2003) 655.
[34] R. Fowler, L.W. Nordheim, Proc. R. Soc. London 119 (1928) 173.
[35] F.G. Tarntair, C.Y. Wen, L.C. Chen, J.J. Wu, K.H. Chen, P.F. Kuo, S.W. Chang, Y.F. Chen, W.K. Hong, H.C. Cheng, Appl. Phys. Lett. 76 (2000) 2630.
[36] C.P. Cho, T.P. Perng, Nanotechnology 18 (2007) 125202.
[37] J.M. Bonard, N. Weiss, H. kind, T. Stöckli, L. Forró, K. Kern, A. Châtelain, Adv. Mater. 13 (2001) 184.
[38] S.K. Patra, G.M. Rao, J. Appl. Phys. 100 (2006) 024319.